Title

Temperature-Dependent Hole Transfer from Photoexcited Quantum Dots to Molecular Species: Evidence for Trap-Mediated Transfer

Journal

ACS Nano, 11(8)

ISSN

1936-0851

Authors

Olshansky, Jacob H
Balan, Arunima D
Ding, Tina X
et al.

Publication Date

2017-08-22

DOI

10.1021/acsnano.7b03580

Peer reviewed

ACSNANO

www.acsnano.org

ARTICLE

Temperature-Dependent Hole Transfer from Photoexcited Quantum Dots to Molecular Species: Evidence for Trap-Mediated Transfer

Jacob H. Olshansky,[†,§,⊥] Arunima D. Balan,[†,§,⊥] Tina X. Ding,[†,§,⊥] Xiao Fu,[†] Youjin V. Lee,[†] and A. Paul Alivisatos*[,†,‡,§,⊥]

[†]Department of Chemistry and [‡]Department of Materials Science and Engineering, University of California, Berkeley, Berkeley, California 94720, United States

[§]Material Sciences Division, Lawrence Berkeley National Laboratory, Berkeley, California 94720, United States

[⊥]Kavli Energy NanoScience Institute, Berkeley, California 94720, United States

Supporting Information

ABSTRACT: The effect of temperature on the rate of hole transfer from photoexcited quantum dots (QDs) is investigated by measuring the driving force dependence of the charge transfer rate for different sized QDs across a range of temperatures from 78 to 300 K. Spherical CdSe/CdS core/shell QDs were used with a series of ferrocene-derived molecular hole acceptors with an 800 meV range in electrochemical potential. Time-resolved photoluminescence measurements and photoluminescence quantum yield measurements in an integrating sphere were both performed from 78 to 300 K to obtain temperature-dependent rates for a series of driving forces as dictated by the nature of the molecular acceptor. For both QD sizes studied and all ligands, the Arrhenius plot of hole transfer exhibited an activated (linear) regime at higher temperatures and a temperature-independent regime at low temperatures. The extracted activation energies in the high-temperature regime were consistent across all ligands for a given QD size. This observation is not consistent with direct charge transfer from the QD valence band to the ferrocene acceptor. Instead, a model in which charge transfer is mediated by a shallow and reversible trap more accurately fits the experimental results. Implications for this observed trap-mediated transfer are discussed including as a strategy to more efficiently extract charge from QDs.

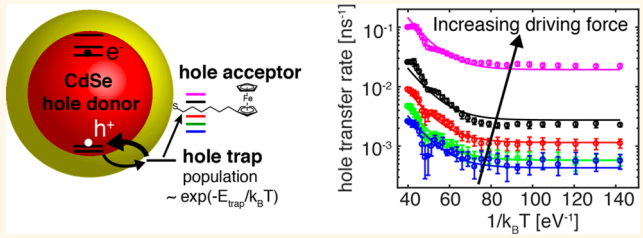

KEYWORDS: *quantum dots, charge transfer, cadmium selenide, hole traps, temperature dependence, ferrocene*

The predominance of the surface in semiconductor nanocrystals, or quantum dots (QDs), presents both desirable and undesirable consequences in advancing QD-based technologies. The proximity of a functionalizable surface to photoexcited charges in QDs allows for efficient and controlled charge extraction, yet ill-defined and undercoordinated surface atoms can also localize these excited charges and nonradiatively dissipate their energy. Charge transfer from QDs to well-defined states is key to a variety of applications that convert solar energy to usable work in the form of chemical energy, such as to produce hydrogen,[1,2] to reduce CO_2,[3,4] or recently to photocatalyze C−C bond formation.[5,6] Alternatively, this work can be converted to electrical energy such as in thin film QD photovoltaics[7,8] or solution junction QD-sensitized solar cells.[9,10] Resultantly, charge transfer from QDs to both molecular[11−13] and bulk states[14−16] has been extensively studied in the past decade.

However, the presence of ill-defined surface states that can participate in charge transfer processes limits the efficiency of controllable extraction of charges from QDs. This has motivated significant work on understanding the chemical and energetic nature of these traps. In cadmium chalcogenide QDs it has been shown that hole traps, typically undercoordinated chalcogen atoms, are more prevalent than electron traps and are the dominant cause of low photoluminescence quantum yields (PLQYs) in these materials.[17−19] Furthermore, temperature-dependent studies of cadmium chalcogenide QDs have demonstrated that this trapping does not necessarily lead to irreversible nonradiative charge recombination. In fact, models that allow for reversible charge trapping to states energetically near the band edge have been shown to reproduce the observed temperature dependence of the photoluminescence (PL).[20−23] Long-lived PL decay components, longer than

Received: May 22, 2017
Accepted: July 31, 2017
Published: July 31, 2017

DOI: 10.1021/acsnano.7b03580
ACS Nano 2017, 11, 8346−8355

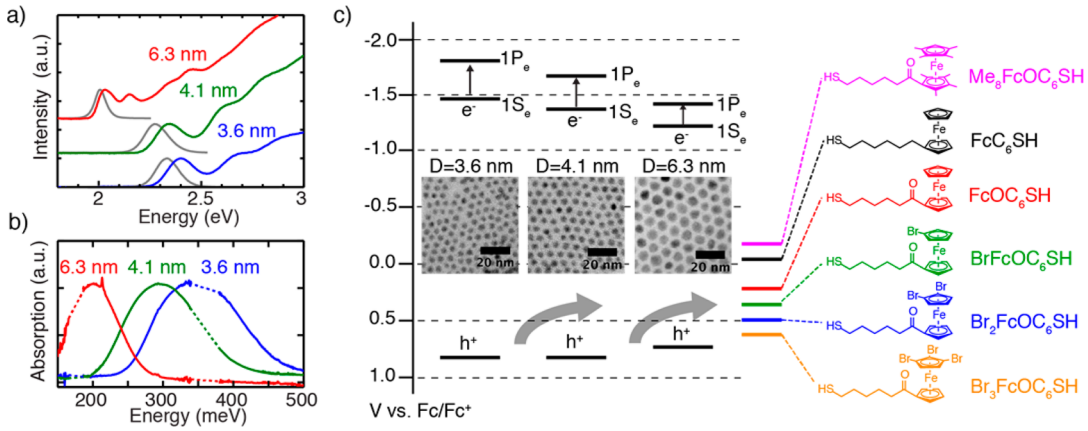

Figure 1. Energetics of the system studied. (a) Absorption and emission (gray) spectra of the 3.6, 4.1, and 6.3 nm QDs. (b) IR intraband absorption spectra of the three QDs after electronic photodoping with lithium triethylborohydride. Dashed sections were removed due to large solvent absorption; see Supporting Information for original spectra. (c) Energy diagram with QD band gaps determined from optical emission and $1S_e-1P_e$ transition energies determined from IR measurements. Ferrocene ligand energies and QD valence band energies were determined in our previous work. TEM micrograph insets for each sample are shown with 20 nm scale bars.

the radiative lifetime, have also been linked to reversible trapping. This delayed fluorescence arises from a restoration of the excitonic state following detrapping and has been shown to persist for as long as milliseconds, following a power law. These results highlight the prevalence of reversible traps, as well as the wide range of detrapping times.[24]

Since these reversible traps do not necessarily lead to nonradiative processes, they can be harnessed to mediate desirable charge transfer if properly understood. A combined experimental and theoretical study by the Wang group and us explored this possibility in a system with a CdSe/CdS rod covalently linked to a hole-accepting ferrocene moiety *via* a thiol bond. The computational work showed the existence of a hole trap associated with the thiol binding head that is ~300 meV below the valence band (energetically uphill) and that this trap can reversibly localize holes as well as mediate hole transfer to the ferrocene. The direct transfer (valence band to ferrocene) was calculated to outcompete this trap-mediated hole transfer, only because the large energy difference between the valence band and trap results in negligible equilibrium population in the trap state. However, if the trap energy is less than ~200 meV below that of the valence band, then the trap-mediated transfer dominates since this process is composed of two short-range charge transfer steps with increased coupling compared to the longer range direct transfer.[25]

We have since constructed an experimental model system based on this work to better understand the mechanism of hole transfer from photoexcited QDs to molecular species. We used spherical core/shell CdSe/CdS QDs with high PLQYs that are covalently linked to hole-accepting ferrocene moieties *via* an alkyl bridge and a thiol binding head, including the ligand used in the computational study. The ability to accurately quantify the number of ferrocene ligands bound per QD *via* ^{1}H NMR allowed us to extract hole transfer rate constants per molecule by monitoring the quenching of the PLQY.[26] Employing this method with six distinct ferrocene-derived hole acceptors with an 800 meV range in energy provided a relationship between driving force and hole transfer rate from photoexcited QDs.[27] The resultant relationship lacked the Marcus inverted region observed in molecular charge transfer processes that involve only two states (initial and final).[28,29] Instead, the hole transfer rate monotonically increased with increasing driving force.

The lack of an inverted region was also observed for electron transfer from photoexcited QDs by the groups of Lian and Prezhdo. They invoked the possibility of Auger-assisted excitation of the residual, nontransferring charge during charge transfer to explain their results.[30,31] In this Auger-assisted Marcus model, an intraband transition allows for multiple final states that reduce the effective driving force and eliminate the inverted region. A number of studies on both hole[32,33] and electron[34] transfer from cadmium chalcogenide QDs to surface traps have also used Auger-mediated models to reproduce experimental observations on trapping dynamics. We employed a similar Auger-assisted model to qualitatively fit our hole transfer relationship.[27] This work assumed direct transfer from the QD exciton to the molecular species. However, trap-mediated transfer through surface states in thermal equilibrium with the excitonic states would be difficult to distinguish from direct transfer. Such transfer would present nearly the same driving forces and could still allow for Auger-assisted transfer.

In this paper we revisit our experimental model system composed of six ferrocene-derived hole-accepting molecules, to probe the presence of trap-mediated charge transfer by measuring the effect of QD size and temperature on hole transfer. We find first that the relationship between driving force and rate is consistent with the Auger-assisted model, without distinguishing between direct and trap-mediated transfer, across a range of QD sizes at room temperature (RT). The temperature dependence of this hole transfer, increasing from 78 K to RT, reveals a consistent Arrhenius slope across all driving forces for a given QD size. This is indicative of indirect hole transfer, and we fit this behavior with a trap-mediated model for hole transfer, extracting energetic information about the relevant hole traps.

RESULTS AND DISCUSSION

We have measured the rate of hole transfer as a function of driving force from varying size CdSe/CdS core/shell QDs to molecular acceptors from cryogenic to room temperature to allow us to observe the presence of trap-mediated charge transfer. We used the same six ferrocene-derived hole-accepting molecules with varying HOMO energies employed in our previous work.[27] The redox potentials of these ligands were controlled *via* functionalization of the cyclopentadiene rings

DOI: 10.1021/acsnano.7b03580
ACS Nano 2017, 11, 8346−8355

with electron-withdrawing (bromine) and -donating (methyl) groups. The structures and naming conventions of the six ferrocene-derived ligands used are shown in Figure 1c.

Room Temperature Hole Transfer. Three different core/shell QD sizes were used for the room-temperature studies with diameters (error) of 3.6 (0.3), 4.1 (0.4), and 6.3 (0.6) nm and were synthesized in accordance with previous work.[36] The 3.6 and 4.1 nm core/shell QDs were both synthesized from 2.2 nm diameter CdSe cores, while the 6.3 nm core/shell QDs were synthesized from 4.3 nm diameter CdSe QDs (see Supporting Information for synthetic details). The three QD samples have band gaps of 2.34, 2.28, and 2.00 eV (smallest size to largest size), as determined by the emission peak, and PLQYs of 19%, 50%, and 45%, respectively (Figure 1a). The moderate PLQYs indicate that significant nonradiative processes are still present at room temperature in these QDs. However, thin shells were used to ensure measurable PLQY quenching of these QDs with a small number (~10) of hole quenchers bound to the surface. The valence band edge positions of the core/shell QDs were derived from the value measured electrochemically in our previous work,[27] adjusted for changes in the band gap of the CdSe core such that one-third of the change in band gap could be attributed to the hole level (due to the ratio of electron and hole effective masses). This approximation assumes that the hole is localized to the CdSe core, and the size of the core dictates the valence band energy. The relative driving force values for each of the ligands are accurate with respect to each other, but a number of assumptions have gone into the valence band energy determination. Most notably, the electrochemical method for determining the band edge energy has been shown to be highly susceptible to systematic errors on the order of 100's of meV depending on solvent, ligand, and even spectator ions.[37] This error will be discussed later, but we believe it does not affect the conclusions of the present work.

The intraband energy spacings in the conduction band were also measured since they are important in implementing the Auger-assisted model for hole transfer from CdSe/CdS core/shell QDs. Recent work by the Gamelin group has demonstrated a facile method for photochemically doping CdSe QDs with excess electrons in the conduction band by using lithium triethylborohydride as a hole scavenger.[38] Steady-state IR absorption spectroscopy of these electronically doped QDs allows for a direct measure of the $1S_e-1P_e$ transitions and therefore provides the energy of the first electronic excited state (Figure 1b). As expected, the $1S_e-1P_e$ transition energy decreased with larger QD diameters with energies of 345, 293, and 201 meV for the three different sized QDs studied. It should also be noted that since the CdSe/CdS conduction band offset is small, the core/shell QDs have reduced $1S_e-1P_e$ energies relative to their corresponding CdSe cores due to electron delocalization into the shell.

In order to reliably prepare solutions of known concentration for both the QDs and ferrocene ligands, extinction coefficients for each species were determined. Inductively coupled plasma atomic emission spectroscopy (ICP-AES) of the Cd concentration of nitric acid-digested QDs coupled with transmission electron microscopy (TEM) sizing data was used to determine the molar extinction for the three QD samples. Quantitative ^{1}H NMR was used to determine molar extinction coefficients of the ferrocene ligands, which had absorption peaks near 440 nm and molar extinction coefficients ranging from 109 to 504 M^{-1} cm^{-1} (see Supporting Information for more details).

Hole transfer rate constants were measured from each of the three QD samples to the six ferrocene derivatives shown in Figure 1c using steady-state PL quenching at RT. For these studies, we found that mixing known concentrations of QDs and a chosen ferrocene ligand at room temperature resulted in rapid and high-yield exchange of the ferrocene ligand on to the surface of the QD as long as the average number of ferrocene ligands per QD was below ~20. ^{1}H NMR was used to characterize the extent of exchange, although on much higher concentration samples than were used for optical studies. Over the range of ligand to QD ratios used for optical studies, both the 3.6 and 4.1 nm QDs exhibited quantitative exchange for thiolated ferrocene ligands added. A small percentage (7−20%) of each ligand addition contained the ferrocene disulfide dimer, which was observed to not participate in exchange (see Supporting Information). The exchange percentages of thiolated ferrocene ligands on the 6.3 nm QDs varied over the range studied (100−70%) and were fit to an equilibrium model to predict the bound fraction of ligand (see Supporting Information). It is worth noting that our previously published work prepared QD−ferrocene conjugates with the additional step of precipitation/resuspension after ferrocene addition to remove excess ligand.[26,27] This is because we used QDs with thicker CdS shells that necessarily required higher surface ferrocene concentrations, well above the ~20 per QD threshold, to achieve measurable PLQY quenching.

In the current work, steady-state quenching was performed on ~0.3 μM QD solutions that were sequentially exposed to aliquots of a solution of a given ferrocene ligand at RT. Steady-state PL spectra were acquired after each ligand addition, thus allowing us to determine the per-molecule hole transfer rate constant, k_{ht}. For a uniform sample of QDs, each with the same number of ligands attached, the PLQY *vs* number bound per QD (N) has been shown to fit the following relation:[26]

$$\mathrm{PLQY} = \frac{k_r}{k_r + k_{nr} + Nk_{ht}} = \frac{\mathrm{PLQY}_0}{1 + N\tau_0 k_{ht}} \quad (1)$$

where k_r, k_{nr}, and $\tau_0 = (k_r + k_{nr})^{-1}$ are the radiative rate constant, nonradiative rate constant, and luminescence lifetime, respectively, for the native QDs. The PLQY of the native QDs is then given by $\mathrm{PLQY}_0 = \tau_0 k_r$. This measurement relies on the assumption that the sole source of PLQY quenching is *via* hole transfer to the ferrocene species. We have no direct evidence of the formation of the oxidized ferrocenium species since the charge recombination involving the more mobile electron is expected to be faster than the initial hole transfer, thus resulting in a state that is too short-lived to be detectable with transient absorption measurements. However, in this work and our previous work, we have ruled out all other possibilities. Energy transfer to ferrocene is precluded due to the minimal spectral overlap of the QD emission with the weakly absorbing ferrocene species, and there is no correlation between the extinction coefficients of the ferrocene derivatives and their quenching ability (FcC_6SH has an extinction coefficient about 3 times smaller than the other derivatives, but also quenches more). Electron transfer is similarly excluded because the ferrocene LUMO is above the conduction band of the QDs. We have also tested the possibility that the ligand exchange process can introduce nonradiative traps independent of the Fc moiety. This possibility was explored in depth in our previous work by using a ligand with a thiol binding head that is not electrochemically active. We found that the ligand exchange

DOI: 10.1021/acsnano.7b03580
ACS Nano 2017, 11, 8346−8355

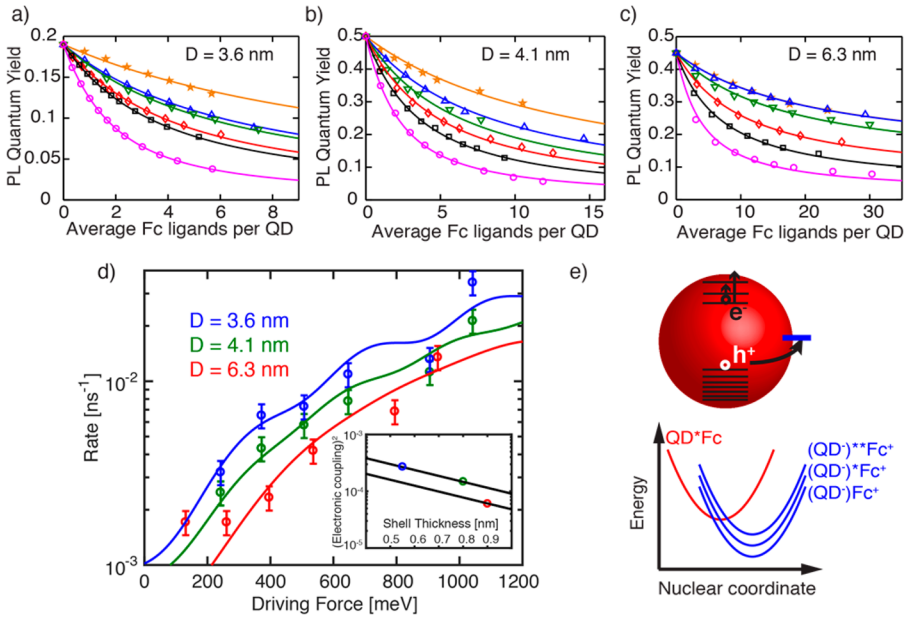

Figure 2. Room-temperature PL quenching of QD−ferrocene conjugates with extracted hole transfer rates. (a−c) PLQY quenching of QDs as a function of the number of ferrocene ligands added. Data points represent experimental measurements, and solid lines are fits using eq 2. Br_3FcOC_6SH (orange, pentagrams), Br_2FcOC_6SH (blue, upward pointing triangles), $BrFcOC_6SH$ (green, downward pointing triangles), $FcOC_6SH$ (red, diamonds), FcC_6SH (black, squares), Me_8FcOC_6SH (magenta, circles). (d) Extracted per molecule hole transfer rates as a function of driving force for each QD size: 3.6 nm (blue), 4.1 nm (green), and 6.3 nm (red). Solid lines represent fits to the data using eq 3. (d, inset) The square of the electronic coupling, extracted from fits to eq 3, as a function of the shell thickness. Solid lines represent fits using the tunneling equation with a damping coefficient of β = 2.4 Å^{-1}. (e) Cartoon of the Auger-assisted mechanism that relies on a series of final charge transfer states accessible *via* electron excitation in the conduction band.

process and the presence of the thiol binding head resulted in an apparent quenching rate about 15 times lower than FcC_6SH.[26] This result is consistent with PLQY quenching studies performed on the 4.1 nm QDs with octanethiol and FcC_6SH. See Supporting Information for further details.

In the current work we are operating in a limit of a few quenchers per QD, much less than in our previous work. We therefore found that employing a Poisson distribution of quenchers produced more adequate fits than eq 1 and instead used the following relation:

$$\mathrm{PLQY}(\langle N\rangle) = \sum_{N=0}^{\infty} \frac{\langle N\rangle^N e^{-\langle N\rangle}}{N!} \frac{\mathrm{PLQY}_0}{1 + N\tau_0 k_{\mathrm{ht}}} \tag{2}$$

where $\langle N\rangle$ is the average number of ferrocene ligands bound per QD. The PL quenching curves for the two smallest QDs (3.6 and 4.1 nm) fit well to this model. See Supporting Information for fits with and without the Poisson distribution. RT quenching data from the 6.3 nm QDs were fit to eq 2 with the $\langle N\rangle$ value adjusted in accordance with the equilibrium model derived from the ^{1}H NMR measurements. RT quenching data are shown in Figure 2a−c.

Fits to the RT quenching data for the 3.6, 4.1, and 6.3 nm QDs to eq 2 produced values for the hole transfer rate constant per molecular acceptor, k_{ht}. In Figure 2d, these values are plotted as a function of the thermodynamic driving force for hole transfer for each of the three QD sizes, clearly exhibiting a monotonic increase in rate with driving force, consistent with our previous work.[27] In this work, we invoked the Auger-assisted model for charge transfer to explain the lack of an inverted region. This model assumes that hole transfer can couple to electron excitation in the conduction band, which allows the rate to stay high at large driving forces. This is because at these driving forces the excess energy lost by the hole is more efficiently transferred to electronic excitation than to nuclear reorganization (a slower process). A schematic of the Auger-assisted model is shown in Figure 2e. There is one initial state composed of the excited QD linked to Fc and multiple final states composed of Fc^+ and the anionic QD^- with varying degrees of intraband electron excitation. The total rate for charge transfer can then be expressed as a sum of the standard nonadiabatic Marcus equation over the multiple states accessed by electron excitation:

$$k_{\mathrm{ht}} = \sum_{i=0} \frac{2\pi}{\hbar} g_{\mathrm{e,i}} |H_{a,b}|^2 \frac{1}{\sqrt{4\pi\lambda k_{\mathrm{b}} T}} \times \exp\left(-\frac{(\lambda + \Delta G_0 + E_{\mathrm{e,i}})^2}{4\lambda k_{\mathrm{b}} T}\right) \tag{3}$$

where $-\Delta G_0$ represents the driving force, $|H_{a,b}|$ is the electronic coupling between donor and acceptor, and λ is the reorganization energy. The effective driving force for each term in the sum is adjusted by the conduction band spacing associated with a given intraband excitation, $E_{\mathrm{e,i}}$. The electronic coupling is assumed to depend strongly on the geometry between the donor and acceptor (QD size, shell thickness, linker length), but only weakly on the degree of electron excitation since it does not significantly alter the delocalization of the electron wave function, so we approximate it as invariant over different electronic final states. This assumption is in accordance with the work by Lian and Prezhdo on Auger-assisted electron transfer from QDs coupled to intraband hole excitation.[30,31] In this combined theoretical and experimental work, the authors found adequate fits to their data by allowing the electronic coupling to be constant with varying degrees of

DOI: 10.1021/acsnano.7b03580
ACS Nano 2017, 11, 8346−8355

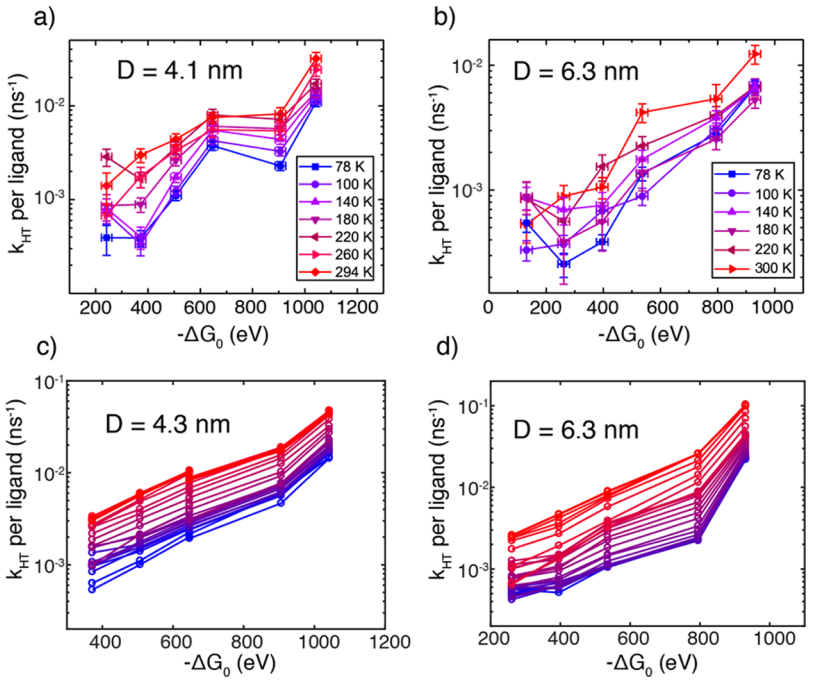

Figure 3. Temperature dependence of hole transfer rates. (a, b) Hole transfer rates extracted from PL lifetime data using eq 4 plotted as a function of both driving force and temperature. The six driving forces shown are determined using the six ferrocene molecules studied. (c, d) Hole transfer rates extracted from temperature-dependent quantum yield measurements performed in an integrating sphere and extracted from eq 5 (using method 1, see Supporting Information for details). These data exclude the lowest driving force ligand, Br_3FcOC_6SH. The temperature range is from 78 K (blue) to 300 K (red).

hole excitation. Figure 2d shows curves constructed using the Auger-assisted model from eq 3 with our measured $1S_e-1P_e$ energies as the values for $E_{e,1}$. Higher energy intraband excitations, such as $1S_e-1D_e$, were also incorporated by using a model for CdSe core QDs developed by Efros and Bawendi.[35,39] This model generated a series of conduction band energy levels, $E_{e,i}$, and associated degeneracies, $g_{e,i}$, given by the spherical harmonics. A full list of these energies and degeneracies is available in the Supporting Information (S8, Table S1).

The reorganization energy was set to 400 meV in these plots. This value for λ is in accordance with previously accepted values for the reorganization energy in these systems.[27,30,40] The inaccuracies associated with the driving force values that were mentioned previously imply that every data point in Figure 2d could be systematically shifted left or right as much as 100 meV. These shifts would partially be accommodated by a different value chosen for the reorganization energy. Nevertheless, the relative magnitudes of the rates for different QD sizes are still interpretable. These differences were explored through the lens of the electronic coupling, the only tunable parameter in fitting these curves. The electronic coupling is expected to be highly dependent on the donor−acceptor distance, d, in accordance with the tunneling relationship: $|H_{a,b}|^2 \propto \exp(-\beta d)$. Our previous work determined that hole transfer through a CdS shell yielded a damping coefficient of $\beta = 2.4$ Å^{-1}.[26] Plotting the square of the electronic coupling *vs* shell thickness (Figure 2d inset) for the three QD sizes is generally consistent with our previously determined damping coefficient (solid lines) for a given core size. The larger core size has a smaller electronic coupling for a given shell thickness, consistent with its predicted smaller surface hole probability density relative to smaller QDs.

The results presented in this section qualitatively provide the same conclusions as in our previously published work.[26,27] These conclusion can be summarized in two points: first, eq 1 can be used over a range of conditions to determine charge transfer rates *via* PLQY quenching, and second the relationship between driving force and rate for hole transfer lacks an inverted region. The current work additionally demonstrates a simpler method for preparing PLQY quenching curves that do not require precipitation/resuspension and quantitative NMR for every data point. This allowed for the collection of driving force *vs* rate curves that could be compared across three different QD sizes, which had not been done in our previous work. It also enabled us to pursue the temperature-dependent rate studies presented in the rest of this paper.

Temperature-Dependent Hole Transfer. Temperature-dependent hole transfer rates were acquired *via* two distinct strategies. First, time-resolved photoluminescence lifetime (TRPL) measurements were performed in an optical cryostat to yield charge transfer rates, and in the second strategy hole transfer rates were determined from temperature-dependent PLQY measurements in an integrating sphere. In the first strategy, hole transfer rate constants, k_{ht}, from the higher PLQY samples (4.1 and 6.3 nm) to each ligand were determined for temperatures between 78 and 300 K using TRPL measurements and eq 4.

$$Nk_{ht}(T) = \tau_{Fc}(T)^{-1} - \tau_0(T)^{-1} \quad (4)$$

where τ_{FC} is the temperature-dependent lifetime of the ferrocene-functionalized QDs and τ_0 is the lifetime of the native QDs. N ranged from 10 to 30 molecules per QD for these experiments. The results are shown in Figure 3a,b. It should be noted that the decay constants at low temperatures (78 or 100 K) did not depend on the range over which the fit

DOI: 10.1021/acsnano.7b03580
ACS Nano 2017, 11, 8346−8355

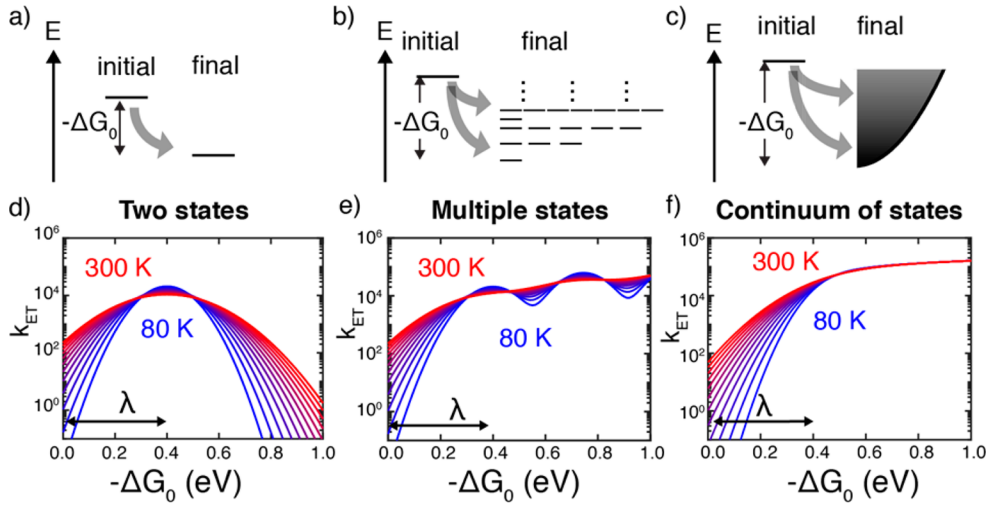

Figure 4. Schematic of the temperature dependence of electron transfer under different formulations of Marcus theory. Energetic diagram of (a) two-state charge transfer, (b) charge transfer with multiple final states such as in eq 3 with the Auger-assisted mechanism, and (c) charge transfer with a continuum of final states. (d–f) Driving force and temperature dependence of charge transfer under the three regimes presented in the top panel. All models assume a reorganization energy of 400 meV.

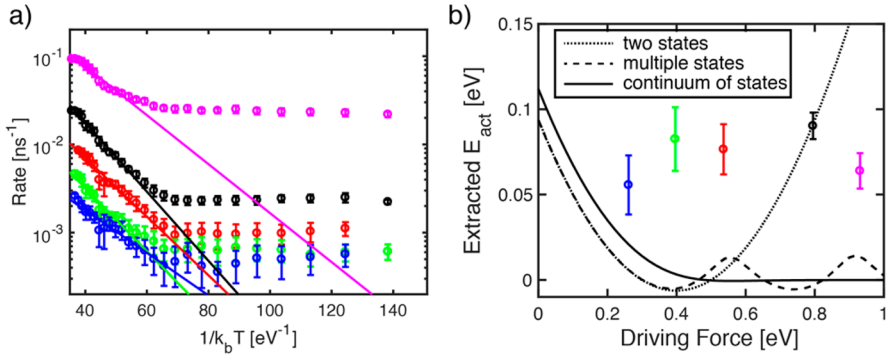

Figure 5. Comparison of the experimental Arrhenius behavior with different versions of Marcus theory. (a) Arrhenius plot of the rate of hole transfer for the five ligands studied *via* temperature-dependent PLQY for the 6.3 nm QDs (the same data as in Figure 3d, but processed using method 2 to better visualize the Arrhenius slope; details are provided in the Supporting Information). Solid lines represent linear fits over the activated regime. (b) Driving force dependence of extracted Arrhenius slopes (effective activation energies) for the experimental data (circles) and for the models presented in Figure 4. Br_2FcOC_6SH (blue), $BrFcOC_6SH$ (green), $FcOC_6SH$ (red), FcC_6SH (black), Me_8FcOC_6SH (magenta).

was performed and, aside from a short rise time, exhibited highly monoexponential decays. At higher temperatures, however, the decays deviate from single exponentials, so the decay constants become dependent on fitting range. We therefore consistently fit over the first decade and accept the associated error. This may result in systematic errors in the value of the rate constants measured at higher temperatures, but relative comparisons between ligands are still valid.

The second strategy for obtaining temperature-dependent hole transfer rates was based on performing PLQY measurements in an integrating sphere. This strategy relies on the fact that the QD emission peak energy is temperature dependent and furthermore is approximately linear in temperature over the 80–300 K range.[41] We could therefore place a 78 K sample into an integrating sphere and record PLQYs while the sample warmed to RT and then use the emission peak energy to determine the corresponding temperature. This process was repeated 5–7 times for each sample to obtain accurate PLQY *vs* temperature data. The temperature-dependent PLQY for native QDs, $QY_0(T)$, and the PLQY for ferrocene-functionalized QDs, $QY_{Fc}(T)$, were used with the following equation to determine the hole transfer rate.

$$Nk_{ht}(T) = \tau_0(T)^{-1}\left(\frac{QY_0(T)}{QY_{Fc}(T)} - 1\right) \quad (5)$$

The results are binned by temperature and shown in Figure 3c,d. Two slightly different methods were used for binning the data and converting the emission energy to temperature. Both methods provided qualitatively similar data; details can be found in the Supporting Information as well as functional fits to the $\tau_0(T)$ data. Due to sample limitations, the 4.1 nm QDs used in the RT and TRPL studies were replaced for a similar sample with a diameter of 4.3 nm and the same sized CdSe core. The same 6.3 nm QD sample was used for all experiments.

There are clearly similarities and differences between the TRPL- and PLQY-derived hole transfer rates. The TRPL data for the 4.1 nm QDs show inverted kinetics at low temperature between the third and second highest driving force ligands ($FcOC_6SH$ and FcC_6SH). It is unclear whether this a manifestation of the discrete nature of the conduction band

DOI: 10.1021/acsnano.7b03580
ACS Nano 2017, 11, 8346–8355

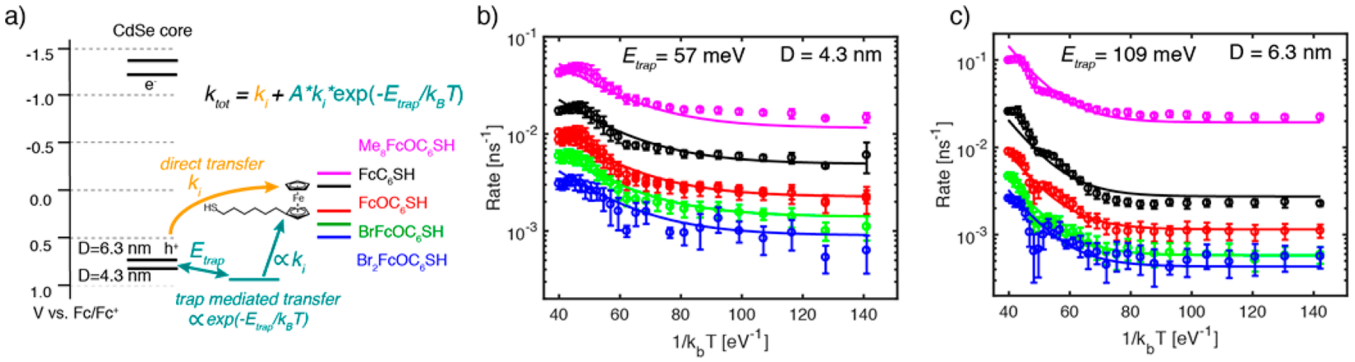

Figure 6. Description of a trap-mediated charge transfer model and fits of this model to the temperature-dependent data. (a) Schematic of the model that assumes the charge transfer rate is a sum of two pathways: direct transfer and trap-mediated transfer. The latter pathway relies on thermal excitation of the hole into a trap of energy E_{trap} relative to the valence band and is therefore temperature dependent. (b, c) Arrhenius plots for the five ferrocene molecules studied on (b) 4.3 and (c) 6.3 nm QDs with fits to the trap-mediated model along with the extracted values for E_{trap}.

states that compose the Auger-assisted model or simply error. Nevertheless, both the TRPL and PLQY data show that the rate decreases by nearly a factor of 10 upon cooling to 78 K. Although the absolute rates differ for each ferrocene ligand, as given by the Auger-assisted model, the temperature dependence appears to be rather consistent. The TRPL data provide coarser data in temperature and were generally susceptible to larger errors due to inconsistencies in fitting the data. We therefore focus the rest of our analysis on the PLQY data shown in Figure 3c,d.

As a point of comparison to our experimental data, we have constructed three different Marcus-based electron transfer models, shown in Figure 4. The first is the standard two-state Marcus model common in molecular systems and exhibiting a clear inverted regime (eq 3 without the summation). The second is a multistate Marcus model, such as the Auger-assisted model, described by eq 3. Finally, a model involving a continuum of final states such as what is observed in bulk systems is also shown. The continuum model employs the standard $E^{1/2}$ dependence of the density of states on energy. It is clear from Figure 4d,e,f that none of these formulations of Marcus theory reproduce the consistent and sizable temperature dependence of the rate across a range of driving forces, as is observed in the experimental data (Figure 3c,d).

To make this comparison clearer, Arrhenius plots of both the experimental data and our Marcus-based models were made. Arrhenius plots for each ferrocene ligand studied on the 6.3 nm QDs are shown in Figure 5a. They all exhibit an activated regime at higher temperatures with extracted activation energies of 60−90 meV depending on the ligand as well as an activationless regime at low temperatures, which will be addressed later. Arrhenius plots for the Marcus-based models (all assumed to be in the activated regime) are provided in the Supporting Information and are nearly linear across all driving forces studied. The slight deviation from linearity comes from the $T^{-1/2}$ factor in the Marcus equation. Activation energies for different values of the driving force were extracted by fitting the Arrhenius plots to lines, and the results are shown with the experimental data in Figure 5b. Clearly, the consistently high activation energies observed in the experimental data do not fit to any single-step Marcus model, which exhibit either low activation energies or driving-force-dependent activation energies.

The consistency in the temperature dependence across all ligands suggests that some process independent of the ferrocene driving force is giving rise to this temperature dependence. We propose that this process is the reversible trapping of holes on the QD surface. As was mentioned in the introduction, reversible traps have been used to explain temperature-dependent PL behavior of QDs, and our previous computational work on CdSe/CdS with FcC_6SH suggested that trap-mediated hole transfer would outcompete direct transfer if the trap was less than 200 meV below the valence band (higher in energy).[40] It should be noted that our measurements are capable of detecting only *reversible* trap-mediated transfer. Irreversible traps, which lead to nonradiative recombination, are accounted for in the k_{nr} rate measured for the native QDs. The extent to which these irreversible traps mediate charge transfer to ferrocene will result in no observed difference between the PLQY of the native QDs and the PLQY of the ferrocene-functionalized QDs, so we cannot measure this charge transfer channel with our current techniques. Reversible trapping, however, allows for band edge PL to persist in the absence of a terminal acceptor such as ferrocene, so reversible trap-mediated charge transfer can be quantified by monitoring loss of PLQY upon the addition of ferrocene acceptors.

On the basis of these observations, we constructed a model that allows for surface trap-mediated hole transfer. Our previous computational work on a CdSe/CdS and FcC_6SH system calculated that direct hole transfer is ∼700 times slower than trapping to a surface sulfur.[40] Additionally, our experimental work with a three-carbon derivative (FcC_3SH) and FcC_6SH suggests that transfer to a surface site would be about 1000 times faster than direct transfer from the core to the Fc moiety (without considering driving force).[26] This large discrepancy in rates allows us to assume that equilibrium can be established between the band edge state and the trap state with relative populations dictated by a Boltzmann factor. To make the model as simple as possible, we assume the existence of a single trap state energy of E_{trap} below the QD valence band (higher in energy). We also assume that the driving force dependence of hole transfer from the trap state will be the same as for the direct transfer, just scaled by some QD-dependent factor, A, that includes some unknown degeneracy of the trap state, as shown in the following equation:

DOI: 10.1021/acsnano.7b03580
ACS Nano 2017, 11, 8346−8355

$$k_{i,\mathrm{tot}}(T) = k_i + Ak_i \exp\left(-\frac{E_{\mathrm{trap}}}{k_{\mathrm{B}}T}\right) \quad (6)$$

where k_i represents the direct transfer rate for ligand i. This model is schematically illustrated in Figure 6a.

Global fits of eq 6 to the data for the 4.3 and 6.3 nm QDs were performed over the five ligands measured to extract values of E_{trap} (Figure 6). The trap energy for the larger QDs is about 50 meV larger than for the smaller QDs. This is approximately the energy difference expected, given the valence band energies of these two different sized QDs, and therefore supports the notion that traps are molecular in nature. That is, the trap energy is not affected by QD size, but as the QD size increases, the E_{trap} value increases in accordance with the changing position of the valence band. The molecular structure of the trap is unknown, but prior work on cadmium chalcogenide QDs would suggest that it is an undercoordinated surface chalcogen species.[17−19,42] For context, our previous work calculated that a fully coordinated thiol species on the surface of a CdSe/CdS nanorod has a HOMO 300 meV below the valence band edge.[40] It is therefore not hard to imagine undercoordinated sulfur species on the QD surface with energies closer to the band edge. Furthermore, there are likely traps deeper within the band gap, possibly further undercoordinated or on specific facets, but our measurement is blind to any of these traps that lead to nonradiative recombination irrespective of the presence of ferrocene (as mentioned previously).

It is worth mentioning how eq 6 reproduces the data and how other versions would also work. In this model, the values for k_i are temperature independent. Therefore, at low temperature when the trap state is not significantly populated, the transfer rate just becomes the temperature-independent k_i. At high temperatures, the faster trap-mediated rate grows proportionally with the trap population, thus reproducing an activated regime. However, k_i should follow Marcus theory and would therefore be moderately temperature dependent itself. Figure 5b suggests that the activation energies are quite low for the multiple state model (*i.e.*, the Auger-assisted model) with driving forces greater than 200 meV, so the temperature dependence of k_i would be rather small. Nevertheless, we constructed a model in which the values for k_i were dictated by the Auger-assisted model (eq 3) and were able to qualitatively reproduce the experimental Arrhenius plots (see Supporting Information). Finally, the presence of an activated and temperature-independent regime could alternatively be explained by a quantized formulation of Marcus theory in which transfer is no longer activated when $k_{\mathrm{B}}T < \hbar\omega$, where ω corresponds to the relevant vibrational frequency for the nuclear rearrangement associated with charge transfer (*i.e.*, the harmonic oscillator frequency for the parabolic potentials shown in Figure 2e).[43] In this case, the Arrhenius slope of the temperature-dependent regime would be dictated by the consistent activation energy of Marcus-based hole transfer to a trap state (rather than a Boltzmann factor). Nevertheless, the conclusion that trap-mediated transfer must be present would not be affected.

The observation of significant trap-mediated transfer necessitates a revised understanding of the room-temperature hole transfer presented in this paper and our previous work, which assumed direct transfer.[26,27] The hole transfer from the trap state to the ferrocene clearly does not exhibit an inverted regime, so a multistate Marcus model would be necessary to fit the behavior. The Auger-assisted model still appears to be a valid way to obtain these multiple states. In this interpretation, the hole transfer from the trap site (rather than direct transfer) to ferrocene is coupled to electron excitation in the conduction band. Alternatively, this hole transfer could be coupled to electron trapping, which would result in the same observed behavior.

This work demonstrates the importance of shallow and reversible traps in QD systems. Their reversibility allows the phooexcited hole to explore a variety of surface sites, thus increasing chances that it will eventually find the target molecular hole acceptor (ferrocene in this case). Our model and previous work[26] suggest that as the shell thickness increases in these QDs, both direct transfer and trap-mediated transfer would be diminished equally. Trap-mediated transfer would likely still dominate, but both would eventually become negligible. Importantly, this work highlights the benefits of designing multistep charge transfer systems that can always be designed to be faster than single-step, longer range, transfer due to the exponential nature of the tunneling efficiency. Further details regarding the molecular nature of these traps would enable the design of more efficient charge separation systems that take advantage of this surface-mediated transfer. The determination of effective trap energies in this paper provides valuable information toward better understanding these electronic states.

CONCLUSIONS

We have expanded on our previous work exploring the driving force dependence of hole transfer from photoexcited QDs using hole-accepting ferrocene-derived ligands. In the current work we examined the effects of QD size and temperature on the relationship between driving force and charge transfer rate. The Auger-assisted model was found to adequately predict the experimental results across a range of three QD sizes. However, the temperature dependence of the hole transfer suggests that the dominant pathway for hole transfer to the ferrocene moiety is *via* a shallow and reversible trap and not *via* direct transfer from the QD excitonic state. This work adds to a growing literature regarding the importance of reversible traps on the excited-state dynamics of QDs. It also demonstrates a method to more efficiently extract charges from QDs since two short-range electron transfer steps are more efficient than a single step. Furthermore, the reversibility of the trapping allows excited charges to persist longer and explore more surface area, thus increasing transfer efficiency to the target species.

METHODS

Synthesis. QDs were synthesized in accordance with previous work.[27,36] A full description of the specific syntheses used in this work is provided in the Supporting Information. The synthesis and characterization of the ferrocene ligands is described in our previous work.[27]

Optical Spectroscopy. Absorption spectra were collected on a Shimadzu 3600 spectrophotometer. Absolute PLQY measurements of native QDs were performed on a custom-built integrating sphere fluorimeter described in previous work.[44] Emission spectra and PLQYs of ligand-exchanged samples were recorded relative to the native QDs on a Horiba Jobin Yvon TRIAX 320 Fluorolog. Steady-state fluorescence quenching curves were performed on 3 mL, ∼0.3 μM, QD solutions in hexanes with 10 μL aliquots of a given ferrocene ligand in toluene added sequentially (each data point in Figure 2a−c represents a ferrocene aliquot addition).

DOI: 10.1021/acsnano.7b03580
ACS Nano 2017, 11, 8346−8355

Photoluminescence lifetime measurements were acquired using a time-correlated single-photon-counting apparatus consisting of a Picoquant Fluotime 300 spectrometer, a PMA 175 detector, and an LDH-P-C-405 diode laser with a 407 nm excitation wavelength. A 1.0 MHz repetition rate was used. Approximately 1 nmol of QDs and 10−20 nmol of ferrocene ligand were dissolved in 0.6 mL of 2,2,4,4,6,8,8-heptamethylnonane (98%, Sigma-Aldrich), an optical glass forming solvent, and were then loaded into a sample cell with two sapphire windows and an inert spacer. The sample cell was placed on a holder within a Janis ST-100 continuous-flow optical cryostat and cooled under flowing liquid nitrogen. The temperature was tuned controllably with a Lakeshore 330 temperature controller.

Temperature-dependent PLQY measurements were performed in flame-sealed NMR tubes containing QD−ferrocene conjugates in 0.4 mL of 3-methylpentane. Tubes were immersed in liquid nitrogen and then quickly transferred to the integrating sphere fluorimeter described above. Spectra were obtained approximately every second for 5 to 10 min to allow the tube to warm to room temperature. This process was repeated as necessary to obtain adequate data.

IR Absorption. Approximately 5 nmol of QDs dissolved in 300 μL of hexanes was combined with 10−50 μL of a THF solution containing 500−2000 nmol of lithium triethylborohydride (Super-Hydride, 1.0 M in THF, Sigma-Aldrich). This solution was kept in an inert, dark environment and loaded into an IR cell with CaF_2 windows and a 500 μM spacer. It was crucial to make sure the cell was impermeable to oxygen and remained dark prior to taking a baseline spectrum on a Bruker IFS 66v/S vacuum FT-IR. The sample was then exposed to light from a UV lamp (365 nm) for 30 s increments prior to acquiring an IR spectrum. The intensity initially increased after each 30 s exposure to UV light, but eventually decreased presumably due to oxidation of the photodoped dots. The peak intensity spectrum was used in the plot in Figure 1b.

ASSOCIATED CONTENT

Supporting Information

The Supporting Information is available free of charge on the ACS Publications website at DOI: 10.1021/acsnano.7b03580.

QD synthetic details; IR absorption spectra; ferrocene ligand optical extinction; ^{1}H NMR quantification of disulfide impurity in Fc ligands and ligand binding studies; PLQY quenching; conduction band energy level calculations; additional characterization methods; temperature dependence of luminescence lifetime; methods for processing temperature-dependent quantum yield data; Arrhenius plots; combined trap-mediated and Auger-assisted model (PDF)

AUTHOR INFORMATION

Corresponding Author

*E-mail: paul.alivisatos@berkeley.edu.

ORCID

Jacob H. Olshansky: 0000-0003-3658-1487

Arunima D. Balan: 0000-0002-9216-7806

A. Paul Alivisatos: 0000-0001-6895-9048

Notes

The authors declare no competing financial interest.

ACKNOWLEDGMENTS

The work was supported by the U.S. Department of Energy, Office of Science, Office of Basic Energy Sciences, Materials Sciences and Engineering Division, under Contract No. DE-AC02-05-CH11231 within the Physical Chemistry of Inorganic Nanostructures Program (KC3103). J.O., T.D., and A.B. acknowledge the National Science Foundation Graduate Research Fellowship under Grant DGE 1106400. A.B. acknowledges support from the Berkeley Graduate Fellowship. The authors acknowledge Son Nguyen and Jianbo Gao for assistance with the optical cryostat and Noah Bronstein for support in obtaining PLQY values.

REFERENCES

(1) Wu, K.; Lian, T. Quantum Confined Colloidal Nanorod Heterostructures for Solar-to-Fuel Conversion. *Chem. Soc. Rev.* **2016**, *45*, 3781−3810.

(2) Amirav, L.; Alivisatos, A. P. Photocatalytic Hydrogen Production with Tunable Nanorod Heterostructures. *J. Phys. Chem. Lett.* **2010**, *1*, 1051−1054.

(3) Manzi, A.; Simon, T.; Sonnleitner, C.; Döblinger, M.; Wyrwich, R.; Stern, O.; Stolarczyk, J. K.; Feldmann, J. Light-Induced Cation Exchange for Copper Sulfide Based CO_2 Reduction. *J. Am. Chem. Soc.* **2015**, *137*, 14007−14010.

(4) Wang, C.; Thompson, R. L.; Ohodnicki, P.; Baltrus, J.; Matranga, C. Size-Dependent Photocatalytic Reduction of CO_2 with PbS Quantum Dot Sensitized TiO_2 Heterostructured Photocatalysts. *J. Mater. Chem.* **2011**, *21*, 13452−13457.

(5) Caputo, J. A.; Frenette, L. C.; Zhao, N.; Sowers, K. L.; Krauss, T. D.; Weix, D. J. General and Efficient C-C Bond Forming Photoredox Catalysis with Semiconductor Quantum Dots. *J. Am. Chem. Soc.* **2017**, *139*, 4250−4253.

(6) Zhang, Z.; Edme, K.; Lian, S.; Weiss, E. A. Enhancing the Rate of Quantum-Dot-Photocatalyzed Carbon-Carbon Coupling by Tuning the Composition of the Dot's Ligand Shell. *J. Am. Chem. Soc.* **2017**, *139*, 4246−4249.

(7) Chuang, C.-H. M.; Brown, P. R.; Bulović, V.; Bawendi, M. G. Improved Performance and Stability in Quantum Dot Solar Cells Through Band Alignment Engineering. *Nat. Mater.* **2014**, *13*, 796−801.

(8) Kramer, I. J.; Sargent, E. H. The Architecture of Colloidal Quantum Dot Solar Cells: Materials to Devices. *Chem. Rev.* **2014**, *114*, 863−882.

(9) Zhao, K.; Pan, Z.; Mora-Seró, I.; Cánovas, E.; Wang, H.; Song, Y.; Gong, X.; Wang, J.; Bonn, M.; Bisquert, J.; Zhong, X. Boosting Power Conversion Efficiencies of Quantum-Dot-Sensitized Solar Cells Beyond 8% by Recombination Control. *J. Am. Chem. Soc.* **2015**, *137*, 5602−5609.

(10) Kamat, P. V. Boosting the Efficiency of Quantum Dot Sensitized Solar Cells Through Modulation of Interfacial Charge Transfer. *Acc. Chem. Res.* **2012**, *45*, 1906−1915.

(11) Knowles, K. E.; Peterson, M. D.; McPhail, M. R.; Weiss, E. A. Exciton Dissociation Within Quantum Dot−Organic Complexes: Mechanisms, Use as a Probe of Interfacial Structure, and Applications. *J. Phys. Chem. C* **2013**, *117*, 10229−10243.

(12) Boulesbaa, A.; Issac, A.; Stockwell, D.; Huang, Z.; Huang, J.; Guo, J.; Lian, T. Ultrafast Charge Separation at CdS Quantum Dot/Rhodamine B Molecule Interface. *J. Am. Chem. Soc.* **2007**, *129*, 15132−15133.

(13) Sykora, M.; Petruska, M. A.; Alstrum-Acevedo, J.; Bezel, I.; Meyer, T. J.; Klimov, V. I. Photoinduced Charge Transfer Between CdSe Nanocrystal Quantum Dots and Ru−Polypyridine Complexes. *J. Am. Chem. Soc.* **2006**, *128*, 9984−9985.

(14) Robel, I.; Kuno, M.; Kamat, P. V. Size-Dependent Electron Injection From Excited CdSe Quantum Dots Into TiO_2 Nanoparticles. *J. Am. Chem. Soc.* **2007**, *129*, 4136−4137.

(15) Žídek, K.; Zheng, K.; Ponseca, C. S.; Messing, M. E.; Wallenberg, L. R.; Chábera, P.; Abdellah, M.; Sundström, V.; Pullerits, T. Electron Transfer in Quantum-Dot-Sensitized ZnO Nanowires: Ultrafast Time-Resolved Absorption and Terahertz Study. *J. Am. Chem. Soc.* **2012**, *134*, 12110−12117.

(16) Cánovas, E.; Moll, P.; Jensen, S. A.; Gao, Y.; Houtepen, A. J.; Siebbeles, L. D. A.; Kinge, S.; Bonn, M. Size-Dependent Electron Transfer From PbSe Quantum Dots to SnO_2 Monitored by Picosecond Terahertz Spectroscopy. *Nano Lett.* **2011**, *11*, 5234−5239.

DOI: 10.1021/acsnano.7b03580
ACS Nano 2017, 11, 8346−8355

(17) Busby, E.; Anderson, N. C.; Owen, J. S.; Sfeir, M. Y. Effect of Surface Stoichiometry on Blinking and Hole Trapping Dynamics in CdSe Nanocrystals. *J. Phys. Chem. C* **2015**, *119*, 27797−27803.
(18) Gao, Y.; Peng, X. Photogenerated Excitons in Plain Core CdSe Nanocrystals with Unity Radiative Decay in Single Channel: the Effects of Surface and Ligands. *J. Am. Chem. Soc.* **2015**, *137*, 4230−4235.
(19) Pu, C.; Peng, X. To Battle Surface Traps on CdSe/CdS Core/Shell Nanocrystals: Shell Isolation *Versus* Surface Treatment. *J. Am. Chem. Soc.* **2016**, *138*, 8134−8142.
(20) Jones, M.; Lo, S. S.; Scholes, G. D. Quantitative Modeling of the Role of Surface Traps in CdSe/CdS/ZnS Nanocrystal Photoluminescence Decay Dynamics. *Proc. Natl. Acad. Sci. U. S. A.* **2009**, *106*, 3011−3016.
(21) Jones, M.; Scholes, G. D. On the Use of Time-Resolved Photoluminescence as a Probe of Nanocrystal Photoexcitation Dynamics. *J. Mater. Chem.* **2010**, *20*, 3533−3538.
(22) Mooney, J.; Krause, M. M.; Saari, J. I.; Kambhampati, P. Challenge to the Deep-Trap Model of the Surface in Semiconductor Nanocrystals. *Phys. Rev. B: Condens. Matter Mater. Phys.* **2013**, *87*, 081201.
(23) Krause, M. M.; Kambhampati, P. Linking Surface Chemistry to Optical Properties of Semiconductor Nanocrystals. *Phys. Chem. Chem. Phys.* **2015**, *17*, 18882−18894.
(24) Rabouw, F. T.; Kamp, M.; van Dijk-Moes, R. J. A.; Gamelin, D. R.; Koenderink, A. F.; Meijerink, A.; Vanmaekelbergh, D. Delayed Exciton Emission and Its Relation to Blinking in CdSe Quantum Dots. *Nano Lett.* **2015**, *15*, 7718−7725.
(25) Tarafder, K.; Surendranath, Y.; Olshansky, J. H.; Alivisatos, A. P.; Wang, L.-W. Hole Transfer Dynamics From a CdSe/CdS Quantum Rod to a Tethered Ferrocene Derivative. *J. Am. Chem. Soc.* **2014**, *136*, 5121−5131.
(26) Ding, T. X.; Olshansky, J. H.; Leone, S. R.; Alivisatos, A. P. Efficiency of Hole Transfer From Photoexcited Quantum Dots to Covalently Linked Molecular Species. *J. Am. Chem. Soc.* **2015**, *137*, 2021−2029.
(27) Olshansky, J. H.; Ding, T. X.; Lee, Y. V.; Leone, S. R.; Alivisatos, A. P. Hole Transfer From Photoexcited Quantum Dots: the Relationship Between Driving Force and Rate. *J. Am. Chem. Soc.* **2015**, *137*, 15567−15575.
(28) Marcus, R. A.; Sutin, N. Electron Transfers in Chemistry and Biology. *Biochim. Biophys. Acta, Rev. Bioenerg.* **1985**, *811*, 265−322.
(29) Miller, J. R.; Calcaterra, L. T.; Closs, G. L. Intramolecular Long-Distance Electron Transfer in Radical Anions. the Effects of Free Energy and Solvent on the Reaction Rates. *J. Am. Chem. Soc.* **1984**, *106*, 3047−3049.
(30) Zhu, H.; Yang, Y.; Hyeon-Deuk, K.; Califano, M.; Song, N.; Wang, Y.; Zhang, W.; Prezhdo, O. V.; Lian, T. Auger-Assisted Electron Transfer From Photoexcited Semiconductor Quantum Dots. *Nano Lett.* **2014**, *14*, 1263−1269.
(31) Hyeon-Deuk, K.; Kim, J.; Prezhdo, O. V. *Ab Initio* Analysis of Auger-Assisted Electron Transfer. *J. Phys. Chem. Lett.* **2015**, *6*, 244−249.
(32) Gómez-Campos, F. M.; Califano, M. Hole Surface Trapping in CdSe Nanocrystals: Dynamics, Rate Fluctuations, and Implications for Blinking. *Nano Lett.* **2012**, *12*, 4508−4517.
(33) Califano, M.; Gómez-Campos, F. M. Universal Trapping Mechanism in Semiconductor Nanocrystals. *Nano Lett.* **2013**, *13*, 2047−2052.
(34) Boehme, S. C.; Azpiroz, J. M.; Aulin, Y. V.; Grozema, F. C.; Vanmaekelbergh, D.; Siebbeles, L. D. A.; Infante, I.; Houtepen, A. J. Density of Trap States and Auger-Mediated Electron Trapping in CdTe Quantum-Dot Solids. *Nano Lett.* **2015**, *15*, 305610.1021/acs.nanolett.5b00050.
(35) Ekimov, A. I.; Kudryavtsev, I. A.; Efros, L.; Al; Yazeva, T. V.; Hache, F.; Schanne-Klein, M. C.; Rodina, A. V.; Ricard, D.; Flytzanis, C. Absorption and Intensity-Dependent Photoluminescence Measurements on CdSe Quantum Dots: Assignment of the First Electronic Transitions. *J. Opt. Soc. Am. B* **1993**, *10*, 100−107.
(36) Chen, O.; Zhao, J.; Chauhan, V. P.; Cui, J.; Wong, C.; Harris, D. K.; Wei, H.; Han, H.-S.; Fukumura, D.; Jain, R. K.; Bawendi, M. G. Compact High-Quality CdSe−CdS Core−Shell Nanocrystals with Narrow Emission Linewidths and Suppressed Blinking. *Nat. Mater.* **2013**, *12*, 445−451.
(37) Boehme, S. C.; Wang, H.; Siebbeles, L. D. A.; Vanmaekelbergh, D.; Houtepen, A. J. Electrochemical Charging of CdSe Quantum Dot Films: Dependence on Void Size and Counterion Proximity. *ACS Nano* **2013**, *7*, 2500−2508.
(38) Rinehart, J. D.; Schimpf, A. M.; Weaver, A. L.; Cohn, A. W.; Gamelin, D. R. Photochemical Electronic Doping of Colloidal CdSe Nanocrystals. *J. Am. Chem. Soc.* **2013**, *135*, 18782−18785.
(39) Norris, D.; Bawendi, M. Measurement and Assignment of the Size-Dependent Optical Spectrum in CdSe Quantum Dots. *Phys. Rev. B: Condens. Matter Mater. Phys.* **1996**, *53*, 16338−16346.
(40) Tarafder, K.; Surendranath, Y.; Olshansky, J. H.; Alivisatos, A. P.; Wang, L.-W. Hole Transfer Dynamics From a CdSe/CdS Quantum Rod to a Tethered Ferrocene Derivative. *J. Am. Chem. Soc.* **2014**, *136*, 5121−5131.
(41) Balan, A. D.; Eshet, H.; Olshansky, J. H.; Lee, Y. V.; Rabani, E.; Alivisatos, A. P. Effect of Thermal Fluctuations on the Radiative Rate in Core/Shell Quantum Dots. *Nano Lett.* **2017**, *17*, 1629−1636.
(42) Houtepen, A. J.; Hens, Z.; Owen, J. S.; Infante, I. On the Origin of Surface Traps in Colloidal II−VI Semiconductor Nanocrystals. *Chem. Mater.* **2017**, *29*, 752−761.
(43) Jortner, J. Temperature Dependent Activation Energy for Electron Transfer Between Biological Molecules. *J. Chem. Phys.* **1976**, *64*, 4860−4867.
(44) Bronstein, N. D.; Yao, Y.; Xu, L.; O'Brien, E.; Powers, A. S.; Ferry, V. E.; Alivisatos, A. P.; Nuzzo, R. G. Quantum Dot Luminescent Concentrator Cavity Exhibiting 30-Fold Concentration. *ACS Photonics* **2015**, *2*, 1576−1583.

DOI: 10.1021/acsnano.7b03580
ACS Nano 2017, 11, 8346−8355